Modeling intra- and intermolecular correlations for linear and branched polymers using a modified test-chain self-consistent field theory

Renfeng Hu and David T. Wu*
Department of Chemical and Biological Engineering and Department of Chemistry, Colorado School of Mines, Golden, Colorado 80401, USA

Dapeng Wang
State Key Laboratory of Polymer Physics and Chemistry, Changchun Institute of Applied Chemistry, Chinese Academy of Sciences, Changchun 130022, People's Republic of China

(Received 18 July 2016; revised manuscript received 25 February 2017; published 13 April 2017)

A modified test-chain self-consistent field theory (SCFT) is presented to study the intra- and intermolecular correlations of linear and branched polymers in various solutions and melts. The key to the test-chain SCFT is to break the the translational symmetry by fixing a monomer at the origin of a coordinate. This theory successfully describes the crossover from self-avoiding walk at short distances to screened random walk at long distances in a semidilute solution or melt. The calculations indicated that branching enhances the swelling of polymers in melts and influences stretching at short distances. The test-chain SCFT calculations show good agreement with experiments and classic polymer theories. We highlight that the theory presented here provides a solution to interpret the polymer conformation and behavior under various conditions within the framework of one theory.

DOI: 10.1103/PhysRevE.95.042502

I. INTRODUCTION

The conformational properties of polymers are of renewed interest with the progress in synthesizing branched polymers with complex architectures [1–12]. Such novel synthesis can strictly control the number of branches and the polymerization degree, e.g., molecules of multiple-armed star [4] and end-branched [5] structures.

Conformations within a single polymer molecule can be strongly influenced by enthalpic interactions, steric repulsions, and conformational entropy, particularly for polymers with a high number of arms emanating from one or multiple branching points. In this case, crowding can lead to stretching of arms near the branch points, resulting in overall swelling of the polymer. The single-molecule conformation can in turn influence how this molecule interacts with surrounding molecules. These intramolecular correlations influence interpenetration and miscibility in the case of blends but can also be expected to influence entanglements and chain dynamics.

The characterization of the correlations in polymer homogeneous solutions and melts has been widely studied using scattering techniques [13–16]. In recent years small-angle neutron scattering (SANS) has extended to polymer micelles, gel networks, and inhomogeneous systems, e.g., copolymers in solution or in blends and polymer blends containing novel nonlinear architectures [17]. In the interpretation of SANS experiments, Gaussian chain conformations for melts are commonly assumed for branched polymers [16,18–20], neglecting the possibility of swelling due to steric crowding.

The polymer conformation is not always Gaussian. In semidilute polymer solutions in good solvent, the polymer conformations undergo a crossover from self-avoiding walk (SAW) to random walk statistics at a length scale corresponding to the blob size ξ [21,22]. In the Daoud and Cotton [23] model for star polymers, the blob size increases with increasing distance from the core to the outside, behaving as an unswollen core and a swollen regime near the core, up to the concentration blob size ξ when the internal concentration matches the solution concentration.

Several molecular simulation studies have been carried out showing the swelling of nonlinear polymers. A molecular dynamics simulation performed by Grest *et al.* [24] indicated that the conformation of arms in a star polymer follows SAW. Recent Monte Carlo simulations [25–27] showed that the backbone of a highly branched comb stiffens and stretches as the side branches become longer and more closely spaced, in general agreement with scaling expectations. Yethiraj [28] performed Monte Carlo simulations for highly branched polymers and concluded that increasing the number or the length of branches without changing the backbone length will increase the stiffness of the backbone significantly, but increasing the side-chain stiffness does not always increase the stiffness of the backbone. A simulation of star polymers in a good solvent [29] also showed that the intramolecular density distribution corresponds to SAW statistics for arm conformation. These excellent simulation works consistently demonstrated that the nonlinear structure can result in swelling and stretching of both polymer backbones and side branches due to crowding effects.

Theories of the conformation of polymer melts and blends have been widely developed. For long-chain polymers, coarse-grained descriptions of the conformations have been successful not only for polymers of varying architectures in the bulk, but also for polymers at interfaces [22,30–35]. In particular, for self-consistent field theory (SCFT), the Gaussian chain model is extended to account for the influence of surrounding chains by a self-consistent mean field. SCFT has enjoyed wide success in explaining the compositional distributions of a wide variety of homogeneous and inhomogeneous polymers [36–39]. However, one drawback of conventional SCFT is that correlations between monomers are only accounted for by the mean field. For highly crowded branched polymers, the correlations become more significant, and it would be desirable

*dwu@mines.edu

FIG. 1. Schematic of linear and branched architectures [5].

to break through the limit of the conventional SCFT to account for such correlations, even in homogeneous systems.

A well-developed method in the study of polymeric bulk thermodynamics is the polymer reference interaction site model (PRISM) theory [40–45]. The PRISM theory solves the liquid polymer system by calculating an integral equation (the PRISM equation) to obtain the intermolecular correlation function. PRISM theory is a general method capable of solving polymeric systems regardless of their architecture. Grayce *et al.* [43] performed PRISM calculations and found swelling of star polymers in both solutions and melts. The stretching of arms was found near the branch point because of the long-range excluded volume effect crowding around the core region. Later, Patil *et al.* [46] studied star and comb polymer melts applying PRISM. Their results indicated that swelling was enhanced with more compact arms or branches. For a long-branched comb with a small number of branches, packing and swelling behaved as a linear chain of the same length as its backbone. However, upon increasing the number while shortening the length of branches, the intermolecular correlation of a highly branched comb was found to be significantly different from the linear chain, exhibiting enhanced swelling similarly to that of a star polymer melt.

In this paper, a test-chain self-consistent field theory algorithm is presented to study the conformations of linear and branched polymers in solutions and melts. The SCFT is applied with an excluded volume potential and extends the theory to an algorithm capturing intra- and intermolecular correlations due to the steric and entropic driving force. Note that a similar but more restricted approach was implemented in a lattice model by Scheutjens and Fleers [47] for a homopolymer by fixing the joint of a star polymer as a grafted monomer at a boundary and calculating the intramolecular density profile in dilute solutions [48,49]. The current study focuses on the swelling of linear and star-branched polymers with the scaling analysis for solutions and melts. The polymers tested are the architecturally symmetric star and linear molecules shown in Fig. 1. We found that the branching can stretch the polymer at short distances from the core and result in an overall swelling conformation of polymers in melts. The calculation of the modified SCFT showed good agreement with many experiments and computations.

II. THEORY AND FORMALISM

A. Scaling theory

Edwards [50] showed that in a semidilute solution, monomers are screened by intermolecular interactions beyond the correlation length, $\xi_E = \sqrt{12v\rho_b}b$, where b is the statistical segment length, ρ_b is the bulk density, and the excluded volume parameter v is positive for repulsive monomer interaction. De Gennes [22] commented that the Edwards correlation length does not reveal the swelling effect of polymers in solutions. The scaling theory for the intramolecular density distributions and the distance from one monomer of a SAW molecule is derived below. We focus on the scaling of the density profile and the excluded volume v. The symbol $\cong$ in the derivation represents a full scaling expression with every variable, and the symbol $\sim$ denotes a scaling relation between two variables.

The scaling law of the monomer density distribution in a single linear chain as a function of the distance from a given monomer can be written

$$\bar{\rho}(r) \cong c\bar{r}^{\alpha}, \tag{1}$$

where $\bar{\rho} = \rho(\bar{r})b^3$ and $\bar{r} = r/b$ are the dimensionless monomer density and distance, respectively. c is independent of $\bar{r}$ and the degree of polymerization N but a function of the dimensionless excluded volume $\bar{v} = vb^{-3}$. The scaling exponent α depends on the single-chain conformation. Particularly, $\alpha = -1$ for an ideal Gaussian chain, and $\alpha = -\frac{4}{3}$ for a swollen chain obeying SAW statistics, which is Edwards' law [51]. The dimensionless size of the molecule, $\bar{R}$, scales as

$$\bar{R} \cong \bar{v}^{\beta} N^{\gamma}. \tag{2}$$

For a single chain with infinite dilute concentration that completely has SAW (i.e., $\alpha = -4/3$), $\beta = 1/5$ and $\gamma = 3/5$, respectively.

The integral of $\bar{\rho}(r)$ over the range of chain length scale $\bar{R}$ is the degree of polymerization N of the chain,

$$N = \int_0^{\bar{R}} \bar{\rho}(\bar{r})d\bar{r}^3 \cong \int_0^{\bar{R}} 4\pi c\bar{r}^{(\alpha+2)}d\bar{r}, \tag{3}$$

which gives

$$c \cong N\bar{R}^{-(\alpha+3)}, \tag{4}$$

where the dimensionless size of molecule $\bar{R}$ must satisfy

$$\bar{R} \cong (\bar{v})^{\beta} N^{\frac{1}{(\alpha+3)}} \tag{5}$$

to guarantee that c is independent of N. Substitute Eq. (5) into Eq. (4) to obtain the general form of the dimensionless prefactor c' as a function of v':

$$c \cong (\bar{v})^{-\beta(\alpha+3)}. \tag{6}$$

Therefore, Eq. (1) can be written as

$$\bar{\rho}(\bar{r}) \cong (\bar{v})^{-\beta(\alpha+3)}\bar{r}^{\alpha} \tag{7}$$

within the length scale of molecule $\bar{R}$. Equation (7) shows the general scaling law for a single chain with a finite excluded volume. For $\bar{v} \to 0$, the intramolecular density profile of the molecule is expected to be the Gaussian random walk. Otherwise Eq. (7) diverges.

The crossover from SAW to random walk occurs when the intermolecular density begins is equal to dimensionless bulk density $\bar{\rho}_b = \rho_b b^3$. The real-chain correlation length $\bar{\xi}_{real}$ is thus defined at a distance where $\bar{\rho}(\xi) = \bar{\rho}_b$. The general form of the correlation length ξ can be written

$$\bar{\xi} \cong (\bar{v})^{\frac{\beta(\alpha+3)}{\alpha}} \bar{\rho}(\xi)^{\frac{1}{\alpha}}. \tag{8}$$

The screening length ξ_{real} for a Flory real chain is given as

$$\bar{\xi}_{\text{real}} \cong (\bar{\rho}_{\text{b}})^{-\frac{3}{4}}(\bar{v})^{-\frac{1}{4}}b, \tag{9}$$

and Eq. (6) reads

$$c \cong (\bar{v})^{-\frac{1}{3}}, \tag{10}$$

which is consistent with de Gennes' derivation [22].

B. Test-chain formalism

The general idea of using SCFT to study the polymer bulk properties originated from the analytical single-chain problem proposed by Edwards [50,51], which involves one chain with a fixed end. The numerical solutions of SCFT basically followed the representation by Helfand for solving inhomogeneous polymer systems. A single chain consisting of N sites with unit Gaussian step length b is first considered. A density propagator called Green's function in a potential $\hat{W}$ observing site t at position $\mathbf{r}$ and site t' at position $\mathbf{r}'$ can be defined as the path integral over all the polymer configurations,

$$G(\mathbf{r},\mathbf{r}';t,t') = \frac{\int \mathcal{D}\mathbf{R}(t)P(\mathbf{R})\exp(-W(\mathbf{R}))\delta(\mathbf{R}(t)-\mathbf{r})\delta(\mathbf{R}(t')-\mathbf{r}')}{\int \mathcal{D}\mathbf{R}(t)P(\mathbf{R})\delta(\mathbf{R}(t)-\mathbf{r})}, \tag{11}$$

where $\mathbf{R}(t)$ is the configuration of the chain as a function of the monomer index t. $P(\mathbf{R}(t))$ is the Gaussian statistics satisfying the Wiener distribution. (The energy unit k_BT is chosen.) For a chain labeled α,

$$P(\mathbf{R}_\alpha(t)) \propto \exp\left[-\frac{3}{2b^2}\int_0^N dt\left|\frac{d\mathbf{R}_\alpha(t)}{dt}\right|^2\right], \tag{12}$$

and the compressible homogeneous interaction energy in terms of the excluded volume effect $\hat{W}$ is given as a functional,

$$\hat{W}[\hat{\rho}(\mathbf{r})] = \frac{v}{2}\int d\mathbf{r}\hat{\rho}(\mathbf{r})^2, \tag{13}$$

where $\hat{\rho}(\mathbf{r})$ is the microscopic density operator defined as

$$\hat{\rho}(\mathbf{r}) = \sum_{\alpha=1}^{n}\int_0^N dt\delta(\mathbf{r}-\mathbf{R}_\alpha(t)). \tag{14}$$

The canonical partition function of the system containing n chains is given by

$$Z = \int\prod_{\alpha=1}^{n}\mathcal{D}\mathbf{R}_\alpha(t)P(\mathbf{R}_\alpha)\exp(-\hat{W}) = \mathcal{Z}_0\int\mathcal{D}\rho\mathcal{D}\mu Q_0^n\exp\left[\frac{-v}{2}\int d\mathbf{r}\rho(\mathbf{r})^2+\int d\mathbf{r}\mu(\mathbf{r})\rho(\mathbf{r})\right], \tag{15}$$

where $\mathcal{Z}_0 = V^n/n!$ (V is the volume of the system). Q_0 is the single-chain partition function in an external field μ. The free energy functional is

$$F[\rho,\mu] = \int d\mathbf{r}\left[\frac{v}{2}\rho(\mathbf{r})^2-\mu(\mathbf{r})\rho(\mathbf{r})\right]-n\ln Q_0[\mu]. \tag{16}$$

Equation (15) can be written in terms of the Green's function defined by Eq. (11):

$$Z = \iint d\mathbf{r}'d\mathbf{r}''G(\mathbf{r}',\mathbf{r}'';N,0) = \iiint d\mathbf{r}d\mathbf{r}'d\mathbf{r}''G(\mathbf{r}',\mathbf{r};t,0)G(\mathbf{r},\mathbf{r}'';N,t). \tag{17}$$

The above integrals are simplified by defining the weight function,

$$q(\mathbf{r};t) = \int d\mathbf{r}'G(\mathbf{r}',\mathbf{r};t,0) \tag{18}$$

and

$$q^\dagger(\mathbf{r};t) = \int d\mathbf{r}''G(\mathbf{r},\mathbf{r}'';N,t), \tag{19}$$

which represent the statistical weight for a chain of t sites starting at the origin to the chain end at $\mathbf{r}$ and the statistical weight of $N-t$ sites starting at $\mathbf{r}$ to the opposite direction, respectively.

The weight functions q and $q^\dagger$ satisfy the modified diffusion equation

$$\frac{\partial q(\mathbf{r})}{\partial t} = \frac{b^2}{6}\nabla^2 q(\mathbf{r})-\mu(\mathbf{r})q(\mathbf{r}), \tag{20}$$

where $\mu(\mathbf{r}) = v\rho(\mathbf{r})$ is the self-consistent mean-field potential by saddle-point approximation, satisfying [36]

$$\frac{\partial F[\rho,\mu]}{\partial\rho} = \frac{\partial F[\rho,\mu]}{\partial\mu} = 0. \tag{21}$$

The monomer density $\rho(\mathbf{r})$ is thus given by

$$\rho(\mathbf{r}) = -\frac{\partial\ln Q_0[\mu]}{\partial\mu}, \tag{22}$$

and it can be evaluated by

$$\rho(\mathbf{r}) = \mathcal{N}\frac{\int_0^N dtq(\mathbf{r};t)q^\dagger(\mathbf{r};t)}{\int_0^\infty d^3\mathbf{r}q(\mathbf{r};N)q^\dagger(\mathbf{r};N)}, \tag{23}$$

where $\mathcal{N}$ is the normalization constant. The integrand of the numerator is the unnormalized density distribution at $\mathbf{r}$. The denominator guarantees that the probability of finding one segment over the volume is 1.

The Laplacian in Eq. (20) is reduced to be radius r dependent only because of the spherical symmetry, which is given as

$$\frac{\partial q(r;t))}{\partial t} = \frac{b^2}{6}\left(\frac{\partial^2 q(r;t)}{\partial r^2}+\frac{2}{r}\frac{\partial q(r;t)}{\partial r}\right)-\mu(r)q(r;t), \tag{24}$$

with boundary conditions $q(r<0;t) = q^\dagger(r<0;t) = 0$ and $\frac{\partial q}{\partial r}|_{r_{\max}} = \frac{\partial q^\dagger}{\partial r}|_{r_{\max}} = 0$, where $r_{\max}$ represents the radius of the system.

Define $q^{\text{fix}}(r;t;t_{\text{fix}})$ and $q^{\dagger\text{fix}}(r;t;t_{\text{fix}})$ as the statistical weight functions of the molecule by fixing the site t_{fix}. The initial conditions are $q^{\text{fix}}(r;0;t_{\text{fix}}) = 1$ and $q^{\dagger\text{fix}}(r;N;t_{\text{fix}}) = 1$. However, when $t = t_{\text{fix}}$, the diffusion along monomers by Eq. (20) is reset to solve $q^{\text{fix}}(r;t>t_{\text{fix}};t_{\text{fix}})$ and $q^{\dagger\text{fix}}(r;t<t_{\text{fix}};t_{\text{fix}})$. The reset initial conditions at t_{fix} must satisfy

$q^{\text{fix}}(r;t=t_{\text{fix}};t_{\text{fix}})=\delta(r)$ and $q^{\dagger\text{fix}}(r;t=t_{\text{fix}};t_{\text{fix}})=\delta(r)$, respectively. Similarly, define $q^{\text{free}}(r;t;t_{\text{fix}})$ and $q^{\dagger\text{free}}(r;t;t_{\text{fix}})$ to represent the statistical weights of one of the free polymers around the fixed chain in the system. The initial conditions for the free molecule are $q^{\text{free}}(r;0;t_{\text{fix}})=1$ and $q^{\dagger\text{free}}(r;N;t_{\text{fix}})=1$.

In bulk polymers, considering multiple chains by fixing t_{fix} of one molecule, the complete SCF potential is therefore

$$\mu(r;t_{\text{fix}})=v(\rho^{\text{fix}}(r;t_{\text{fix}})+\rho^{\text{free}}(r;t_{\text{fix}})), \tag{25}$$

where ρ^{fix} is the intramolecular density of the chain selected to hold t_{fix} at the origin, and ρ^{free} is the density distribution of all free molecules The intramolecular monomer density distribution of the fixed chain from site t_{fix} is thus written as

$$\rho^{\text{fix}}(r;t_{\text{fix}})=\frac{\int_0^N dt\; q^{\text{fix}}(r;t;t_{\text{fix}})q^{\dagger\text{fix}}(r;t;t_{\text{fix}})}{4\pi\int_0^{r_{\max}} dr\; q^{\text{fix}}(r;N;t_{\text{fix}})q^{\dagger\text{fix}}(r;N;t_{\text{fix}})r^2}, \tag{26}$$

and the intermolecular density $\rho^{\text{free}}(r;t_{\text{fix}})$ is

$$\rho^{\text{free}}(r;t_{\text{fix}})=\frac{\rho_b V}{N}\frac{\int_0^N dt\; q^{\text{free}}(r;t;t_{\text{fix}})q^{\dagger\text{free}}(r;t;t_{\text{fix}})}{4\pi\int_0^{r_{\max}} dr\; q^{\text{free}}(r;N;t_{\text{fix}})q^{\dagger\text{free}}(r;N;t_{\text{fix}})r^2}, \tag{27}$$

where ρ_b is the bulk monomer density.

The calculation of the density propagators of a branched structure is referenced by Fredrickson [37]. Taking a three-arm structure, with the arms labeled 1, 2, and 3 as an example, t_{fix} is located on arm 3. $q1(r;t;t_{\text{fix}})$ diffuses from the end of arm 1, and $q1^{\dagger}(r;t;t_{\text{fix}})$ diffuses towards the end of arm 1. $q2$ and $q3$ diffuse from the end of arms 2 and 3, respectively. At t_{joint}, $q1^{\dagger}(r;t_{\text{joint}};t_{\text{fix}})$ is given as $q1^{\dagger}(r;t_{\text{joint}};t_{\text{fix}})=q2(r;t_{\text{joint}};t_{\text{fix}})q3(r;t_{\text{joint}};t_{\text{fix}})$. A brief illustration of propagating q and $q^{\dagger}$ is given in Fig. 2.

The SCF calculation is iterated by solving Eqs. (24)–(27), including two sets of modified diffusion equations to solve the fixed- and free-chain statistical weight functions. The segment length b is set to be 1 to keep the results in dimensionless units. The Crank-Nicolson algorithm is used to solve the differential equations, and the Picard algorithm is applied in the SCF iteration by updating μ^i. A mixing ratio $\lambda=0.05$ ($\lambda\in(0,1]$) is applied to update μ^i in terms of $\mu^i=(1-\lambda)\mu^{i-1}+\lambda v\rho^i(r)$. Minimize $\epsilon=\frac{\sum_j|\mu_j^i-\mu_j^{i-1}|}{\sum_j|\mu_j^i|}$ until the tolerance of the convergence $\epsilon_t<10^{-7}$ is satisfied, where i is the index of the ith iteration and j is the index of the spatial grids.

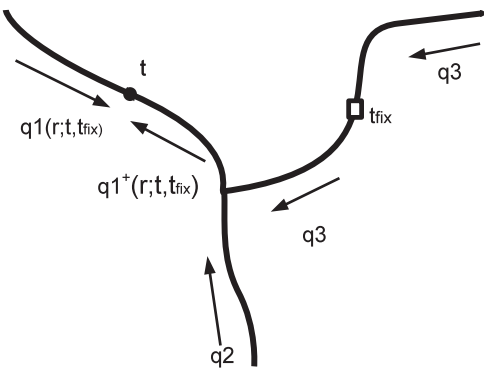

FIG. 2. Illustration to calculate the local density probability of a three-arm structure. In this example, the molecule is fixed at t_{fix}. As $q3$ is solved from the end of the chain and reaches t_{fix}, $q3$ is reset to an initial condition, $q3(r;t=t_{\text{fix}};t_{\text{fix}})=\delta(r)$.

III. RESULTS AND DISCUSSION

A. Dilute solution of linear and star polymers

A single linear chain of $N=50$ in a dilute solution is studied using test-chain SCFT. Equations (7) and (8) indicate that the molecular weight N does not influence the scaling of the density and ξ. The resolution of the discretization grids is $\Delta r=0.02b$ unless otherwise specified. The excluded volume parameter $\bar{v}$ ranges from 0 to 100. $\bar{v}$ is dependent on the compressibility [33]. In Fig. 3(a), the monomer density profiles show the real-chain scaling of $-4/3$ if $\bar{v}$ is sufficiently large as a result of the center of the molecule's being fixed at the origin. The density profiles when $\bar{v}\lesssim 0.1$ show less steep slopes, indicating that the weak excluded volume effect does not exhibit swelling. The plot for $\bar{v}=0$ is very close to $\bar{v}=0.01$

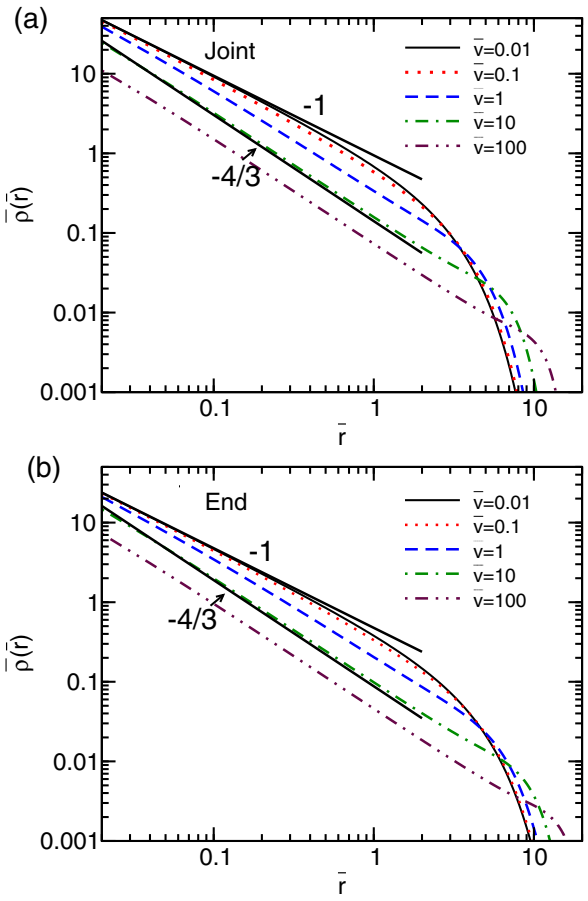

FIG. 3. Intramolecular density profiles of a linear single molecule for different values of excluded volume $\bar{v}$ on log-log scales. (a) Intramolecular density profiles of a linear molecule from the center. (b) Intramolecular density profiles of a linear molecule from the end. The length of the molecule $N=50$.

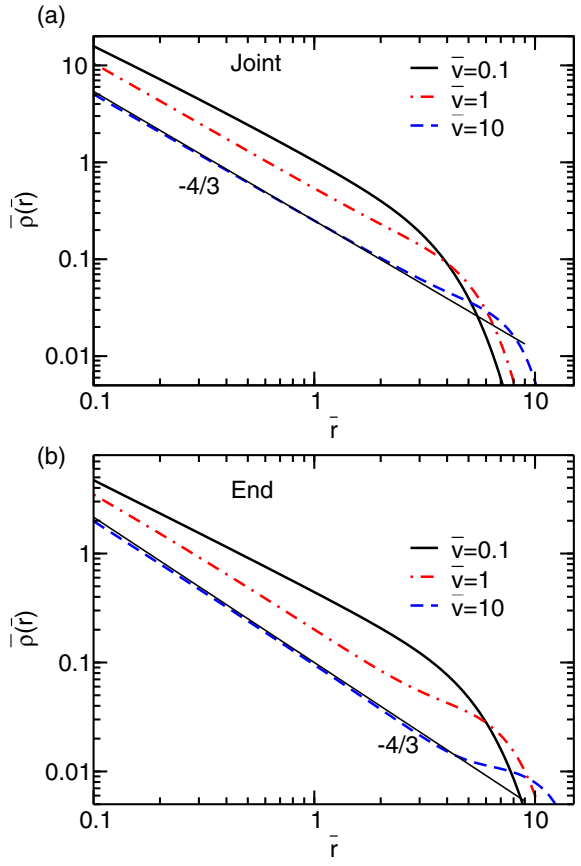

FIG. 4. Intramolecular density profiles of a 4-star polymer with $N_{\text{arm}} = 25$ for different values of excluded volume $\bar{v}$ calculated (a) from the joint and (b) from the end.

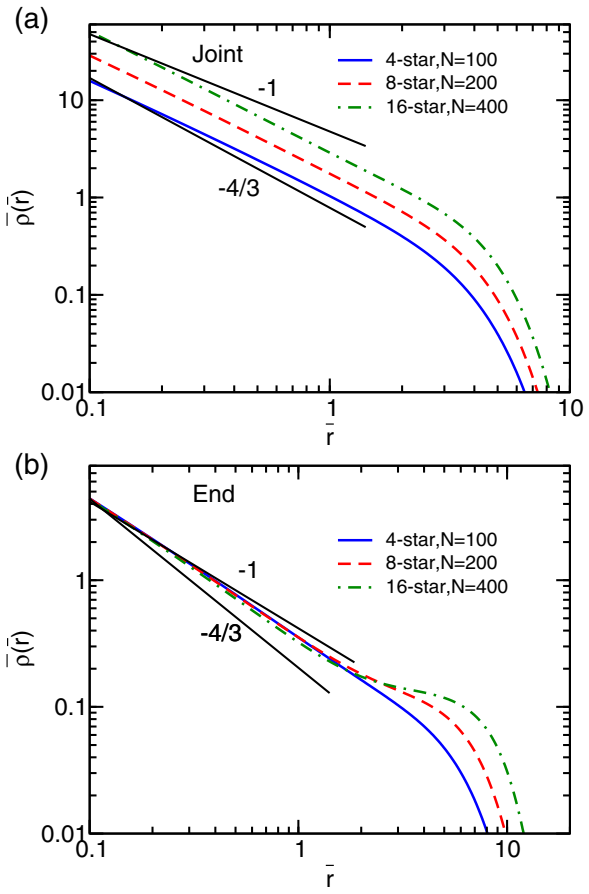

FIG. 5. Density distributions of f-star $N_{\text{arm}} = 25$ and $\bar{v} = 0.1$ under a dilution solution condition calculating from (a) the joint and (b) the end, respectively. $N_{\text{arm}} = 25$, $N_{\text{star}} = 100$.

and indistinguishable from this scale, reflecting a Gaussian conformation with a slope close to 1. In the cases of $\bar{v} \gtrsim 1$, the density profiles indicate that the polymer conformation becomes swollen and the slope of the single-chain density profile is very close to $-4/3$ within the range of the plot when $\bar{v} = 10$. Another feature of the strong excluded volume is that the slope changes at the length scale of R, which is likely due to weaker correlations farther from the center of mass. For $\bar{r} \to 0$, the molecule should always be SAW because a monomer with a finite excluded volume does not interact with other monomers. However, due to the finite grid size, this limit is not captured by the calculation. The density profiles from the held-end monomer of the same linear chain is plotted in Fig. 3(b). The scaling exponent is analogous to that of holding the center. Its slope, close to $-4/3$, indicates the swelling of the molecule in a dilute solution for $\bar{v} \gtrsim 10$, and the slope close to -1 for $\bar{v} \lesssim 0.1$ indicates the Gaussian conformation. The magnitude of the density from the end monomer scales as 1/2 compared to the density from the center [Fig. 3(a)] because the accumulative density from the end is only half that from the center.

A further study of star molecules in dilute solutions is performed using the model of a 4-star with the arm length $N_{\text{arm}} = 25$ and $N = 100$. Density profiles results analogous to those in the case of a single linear molecule from the joint and the end are shown in Figs. 4(a) and 4(b), respectively. For $\bar{v} = 0$, the density profile is also indistinguishable from the plot of $\bar{v} = 0.01$. The slope of $\rho(r)$ from the joint, similar to that of a linear molecule, implies that the conformation is similar to a SAW when $\bar{v} \gtrsim 1$. Figure 4(b) shows that the molecule density from the held end behaves completely as a SAW when $\bar{v} = 10$ until the monomers are near the joint at a length scale of R. Thus, a small increase in density is present at long distances from the center. The scaling exponent of the SCFT agrees with the scaling theory for linear polymer solutions [22] and Monte Carlo simulations of star polymers demonstrated in Ref. [29].

A series of f-stars with identical arm lengths $N_{\text{arm}} = 25$ were computed. The density distributions are shown in Fig. 5. The density profiles from the joint of an f-star shown in Fig. 5(a) are similar to the profiles of the 4-star. The scaling exponent of the density profiles when $\bar{v} = 0.1$ is intermediate between $-4/3$ and -1, reflecting partial swelling. This indicates that the number of arms does not impact the local swelling of a polymer in dilute solutions. However, the number of arms has an influence at long distances. For example, Fig. 5(b) shows the density profiles from the ends of a polymer with an increased number of arms. The scaling exponent of the density of the 16-star increases and then plateaus with a slope close to 0 where the end monomer sees the accumulative density of the joint. This shows a good agreement with SANS results on the size of star polymers [52].

B. End-to-end distance distribution

The end-to-end distance can be generated straightforwardly in the test-chain SCFT algorithm by holding one chain end fixed. In SCFT, the distributions of the distance between two ends can be written in terms of $q(r;N;0)$, which is the statistical weight, by holding the end 0 and diffuse to the other end N. Thus, the three-dimensional normalized end-to-end distance distribution is

$$P(r) = \frac{q(r;N;0)}{4\pi \int_0^\infty q(r;N;0) r^2 dr}. \tag{28}$$

The SCFT result reduces to an exact Gaussian chain without the mean field. When the excluded volume effect is applied, the distribution function becomes a real-chain type and is comparable with the des Cloizeaux form [53],

$$P(r) \cong \left(\frac{r}{\sqrt{\langle R^2\rangle}}\right)^{\sigma} \exp\left(-G\left(\frac{r}{\sqrt{\langle R^2\rangle}}\right)^{\tau}\right), \tag{29}$$

where the exponents and prefactors can be estimated [54,55] as

$$P(r) \approx 0.278 \langle R^2\rangle^{-3/2} \frac{r}{\sqrt{\langle R^2\rangle}}^{0.28} \exp\left(-1.206\left(\frac{r}{\sqrt{\langle R^2\rangle}}\right)^{2.43}\right) \tag{30}$$

for a Flory real chain. The mean square end-to-end distance $\langle R^2\rangle$ is given by

$$\langle R^2\rangle = 4\pi \int_0^\infty P(r) r^4 dr. \tag{31}$$

Figure 6 provides the SCFT results of the monomer end-to-end distribution profiles of the linear ($N = 100$) and 4-star ($N = 100$) molecule in dilute solutions. As shown in Fig. 6(a), with increasing $\bar{v}$, the linear chain becomes non-Gaussian and narrowly distributed. The des Cloizeaux plot is close to the SCFT plot with $\bar{v} = 1$. The end-to-end distribution profiles for strong repulsive polymers $\bar{v} \gtrsim 10$ show that the ends are distant close to $\sqrt{\langle R^2\rangle}$. However, the same calculation for a 4-star with $\bar{v} = 100$ in Fig. 6(b) shows that the end-to-end distribution is wider than a linear chain having the same degree of polymerization.

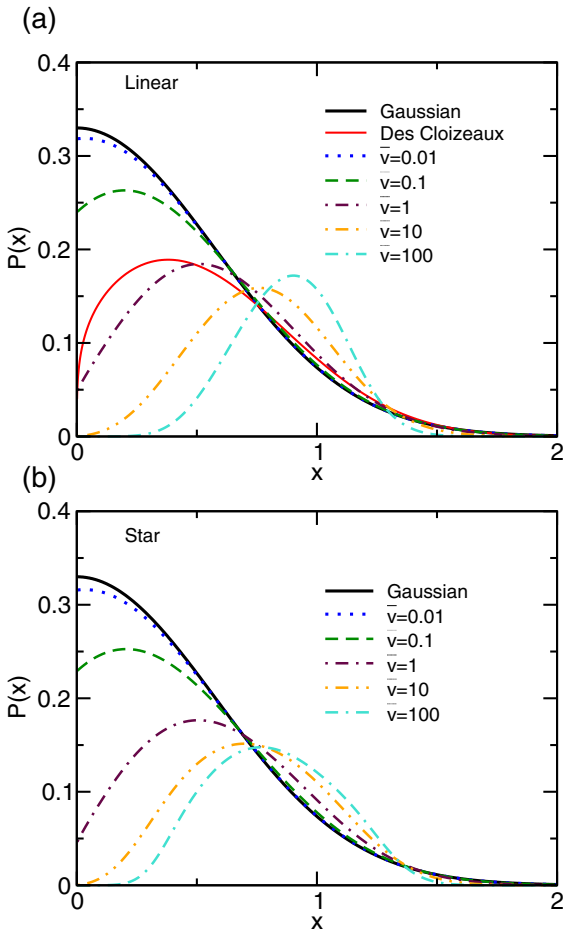

FIG. 6. Single-chain end-to-end distribution function of (a) a linear molecule ($N = 50$) and (b) a 4-star ($N = 100$) by SCFT as a function of the reduced distance $x = \frac{r}{\sqrt{\langle R^2\rangle}}$. The Gaussian model is also provided for comparison.

C. Semidilute solution and polymer melts

1. Density distribution functions

The test-chain SCFT can help us to understand the conformations of linear and nonlinear polymers in a semidilute or concentrated solution as well. As the density becomes finite, chains are screened due to intermolecular interactions. Equation (9) nicely captures a crossover in the scaling exponent from self-avoiding to random walk, indicating that the intermolecular interaction dominates at long distances. The SCFT calculations are performed in a linear solution with a finite density. The degree of polymerization of the linear molecule is $N = 50$ and the reduced average bulk monomer density $\bar{\rho}_b = \rho_b b^3$, which is defined by the total number of monomers over the volume, is variable. The excluded volume parameter $\bar{v}$ is variable as well.

The intra- and intermolecular density profiles of linear polymers in semidilute solutions ($\bar{\rho}_b = 0.2$) as a function of the excluded volume parameters $\bar{v}$ from the joint and end are shown in Fig. 7. The intramolecular density profiles show different scaling exponents in the low-$\bar{r}$ regime at approximately $\bar{r} \lesssim 2$ in the figure. They cross over at $\bar{r} \approx 3$ and merge at $\bar{r} \gtrsim 5$ in the range of the plot. A "correlation hole" is obtained in the plot of the intermolecular concentration profile. For $\bar{v} = 100$, fewer monomers approach the short-distance regime ($\bar{r} \approx 1$) for the strong repulsion due to the monomer excluded volume.

Figure 8(a) shows the intramolecular densities of a linear polymer with $N = 50$, $\bar{\rho}_b = 0.2$, and varying excluded volumes. In homogeneous solutions, the overlap concentration is $c^* \cong N^{-4/5} b^{-3}$ for chains in SAW. The bulk density of $\bar{\rho}_b = 0.2$ in Fig. 8(a) refers to a concentration above the limit of the semidilute solution because c^* is $\sim O(10^{-2}) b^{-3}$. Again, the calculations show that the monomer density decreases as the strength of the monomer exclusion $\bar{v}$ increases.

For solutions with a small excluded volume (e.g., $\bar{v} < 0.01$), the molecule behaves as a Gaussian random walk. This is the same as the single-chain conformation in dilute solutions. Moreover, increasing $\bar{v}$ from 0.01 to 1, a partially screened regime can be obtained [Fig. 8(a)]. Although the complete

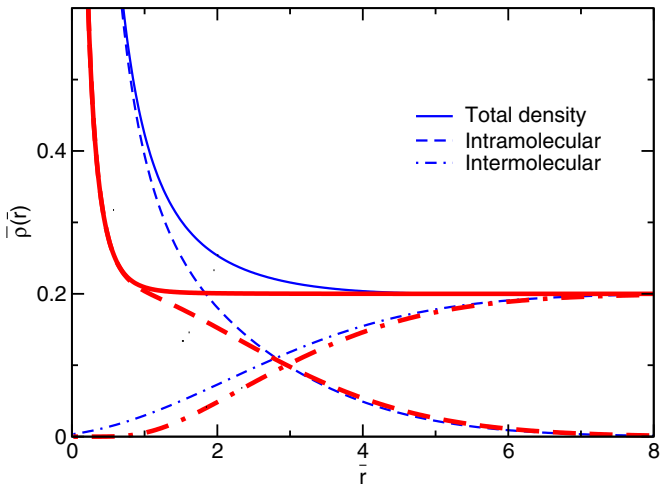

FIG. 7. Density profiles of a linear polymer with $N = 50$ and $\bar{\rho}_b = 0.2$ in melts. The thin solid, dashed, and dash-dotted lines correspond to the total, intramolecular, and intermolecular density profiles with $\bar{v} = 1$, respectively. The thick solid, dashed, and dash-dotted lines are the total, intramolecular, and intermolecular density profiles with $\bar{v} = 100$, respectively.

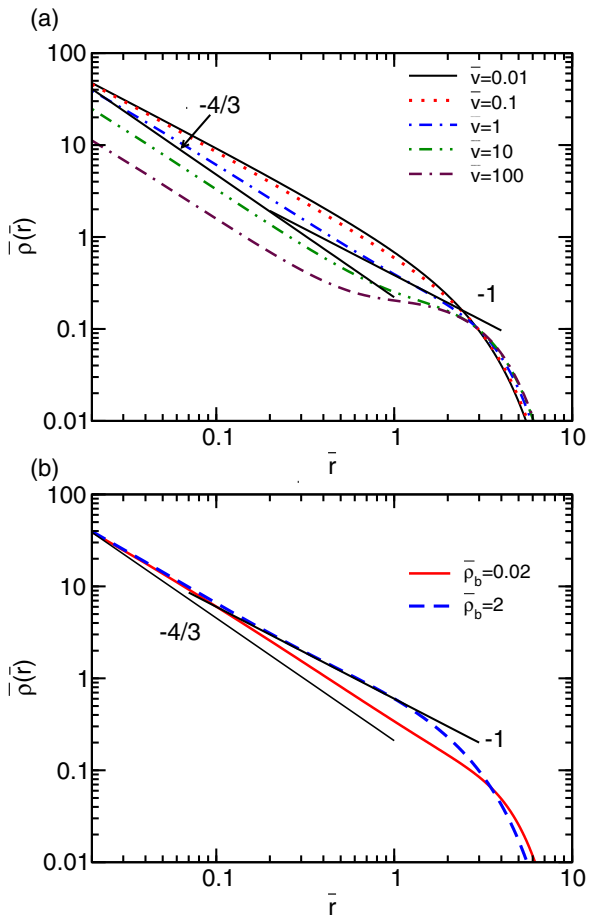

FIG. 8. Intramolecular density profiles for linear polymers in various solutions. (a) $\bar{\rho}_b = 0.2$; $\bar{v}$ varies from 0.01 to 100. The slope of the density profile on the log-log scales is between $-4/3$ and -1 at $\bar{r} \approx 0.1$. (b) $\bar{v} = 1$; $\bar{\rho}_b$ varies from 0.02 to 2.

SAW scaling exponent, $-4/3$, within the blob [22] is not captured by the test-chain SCFT, the calculation is still expected to yield SAW at $\bar{r} \to 0$. In the current resolution ($\Delta\bar{r} = 0.02$), at short distances from the origin where $\bar{r} \approx 0.1$, the density profile has a transitional exponent between $-4/3$ and -1 and the profiles merge to the Gaussian random walk exponent, -1, at long distances. However, the random walk regime is vanishing as $\bar{v}$ approaches 100. In particular, the intramolecular density profile of $\bar{v} = 100$ does not show a random walk slope of -1 but a higher density in the bulk on log-log scales. This is due to the strong repulsion among monomers. If the bulk concentration is increased while fixing the excluded volume, as shown in Fig. 8(b), the screening of the molecules can therefore still be captured at a higher concentration. When $\bar{r}$ goes to 0, the intramolecular density profiles will merge regardless of the value of the bulk densities.

2. *Scaling analysis*

In this section, we discuss the scaling of the excluded volume in the intramolecular density profile at short distances, $\bar{\rho}(\bar{r}) \sim \bar{r}^{\alpha}\bar{v}^{-\beta(\alpha+3)}$. The plot of $\bar{\rho}(\bar{r})/\bar{r}^{\alpha}$ vs $\bar{v}$ is shown in Fig. 9(a) at distances $\bar{r} < 0.1$. The bulk density remains constant, $\bar{\rho}_b = 0.2$. When $\bar{v} \leqslant 0.01$, $\alpha = -1$, and when $\bar{v} \geqslant 1$, $\alpha = -4/3$, according to the discussion of Fig. 8(a). In particular, two regimes for $\bar{\rho}(\bar{r})/\bar{r}^{\alpha}$ vs $\bar{v}$ at log-log scales are identified. When $\bar{v} \leqslant 0.01$, $\bar{\rho}(\bar{r})/\bar{r}^{\alpha}$ is independent of $\bar{v}$. However, when $\bar{v} > 1$, the scaling relationship between the monomer density and the distance shows that $\bar{\rho}(\bar{r})/\bar{r}^{\alpha} \sim (\bar{v})^{-1/3}$, which is consistent with Eq. (10) as a SAW chain. The two regimes cross over within the range $0.01 < \bar{v} < 1$.

The scaling analysis based on expressions from Eq. (1) to Eq. (10) primarily assumes that at short distances, the intramolecular density profile in a melt is the same as it is in dilute solutions. This assumption is true at $\bar{r} \leqslant 0.1$ in the SCFT calculations above, because the total monomer density at short distances is dominated by the intramolecular density (Fig. 7). However, significant differences are seen at long distances in melts with strong excluded volumes when comparing Fig. 3(a) and Fig. 8(a). As shown in Fig. 9(b), we found that $\bar{\xi}$ also crosses over at approximately $\bar{v} = 1$ but the slope for $\bar{v} > 1$ is $-1/8$. This is only half the expected scaling exponent, $\bar{\xi} \sim \bar{v}^{-1/4}$, according to Eq. (9). Applying the intramolecular density profiles in dilute solutions, shown by the crosses in Fig. 9(b), the plot of $\bar{\xi}$ vs $\bar{v}$ shows the scaling exponent of $\bar{\xi} \sim \bar{v}^{-1/4}$. The inset in Fig. 9(b) shows the difference in the screening lengths determined from intramolecular density profiles in a dilute solution vs a melt. In the inset, a difference in conformation is shown in the regime $\bar{\rho}(r) \approx \bar{\rho}_b$ between the dilute and the semidilute solutions. In particular, the single chain must maintain SAW at $\bar{\xi}$, but the chain conformation of the semidilute solution with $\bar{\rho}_b = 0.2$ becomes non-SAW at much shorter distances than $\bar{\xi}$. The existence of both SAW and Gaussian random walk within $\bar{\xi}$ by SCFT leads to a weaker scaling exponent, $-1/8$, than the scaling theory, $-1/4$. Moreover, the crossover from weak v dependence to strong v dependence in Fig. 9 is consistent with the expected criteria of observing SAW using the z parameter,

$$z = \frac{3}{2\pi}^{3/2} \frac{v}{b^3} N^{1/2} \approx \frac{v}{b^3} N^{1/2}, \tag{32}$$

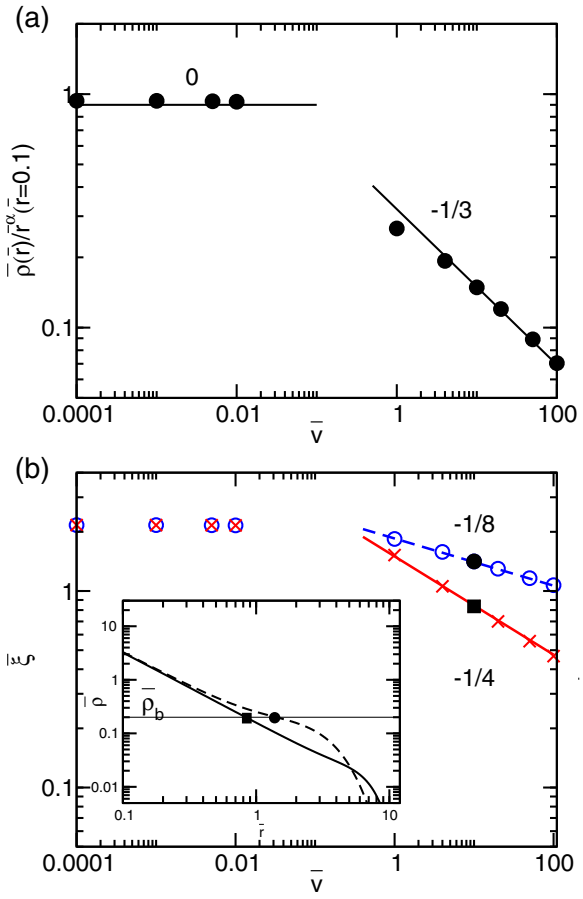

FIG. 9. Scaling analysis of the monomer density and correlation lengths versus the excluded volume in concentrated solutions and melts of linear polymers. (a) Scaling dependence of the scaled monomer density $\bar{\rho}(\bar{r})/\bar{r}^{\alpha}$ on the excluded volume $\bar{v}$ at $\bar{r} = 0.1$ in solutions with $\bar{\rho}_b = 0.2$ and $N = 50$. (b) Scaling dependence of correlation lengths $\bar{\xi}$ on $\bar{v}$ in solutions. Circles are obtained from the intramolecular densities of solutions in Fig. 8(a). Crosses are obtained assuming that the intramolecular density profile in a melt is the same as in the dilute solution (Fig. 3). Inset in (b): The way to obtain $\bar{\xi}$, where $\rho(\bar{\xi}) = \bar{\rho}_b$, from the intramolecular density profiles. Dashed line: $\bar{v} = 10$, $\bar{\rho}_b = 0.2$. Solid line: a dilute solution with $\bar{v} = 10$.

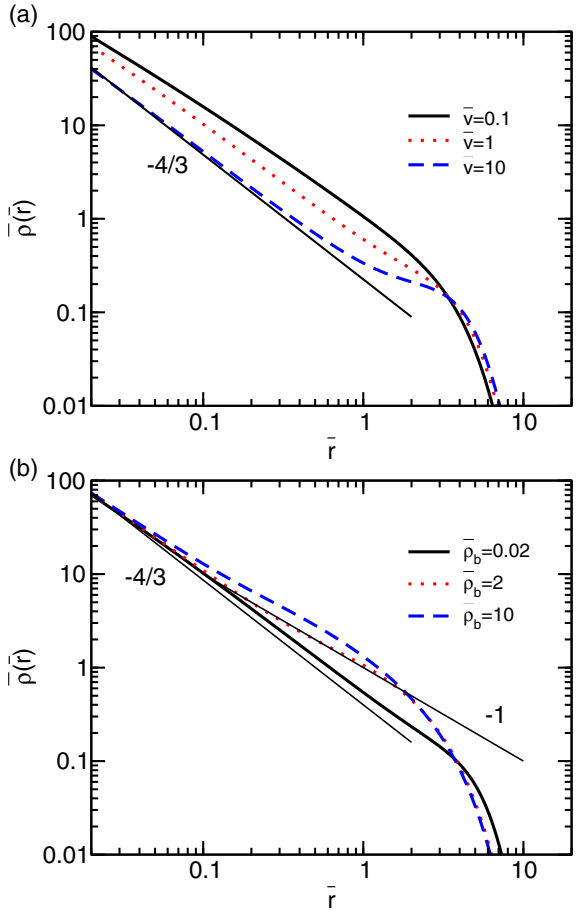

FIG. 10. Density profiles from the joint of 4-star chains with $N = 100$. (a) $\bar{\rho}_b = 0.2$ and $\bar{v}$ varies. (b) $\bar{v} = 1$ and $\bar{\rho}_b$ varies.

where the actual excluded volume, $v \approx b^3$, is the limit of observing SAW at a given N.

3. *Swelling of star polymers in semidilute solutions and melts*

Homogeneous melts composed of 4-star ($N = 100$) molecules with different $\bar{\rho}_b$ and $\bar{v}$ are studied. In general, the behavior of the star-polymer conformation is found to be similar to that of the linear ones with $N = 50$ (a linear is equivalent to a 2-star from the center as shown in Fig. 1). Figures 10(a) and 10(b) compare the intramolecular density profiles by varying $\bar{v}$ and $\bar{\rho}_b$, respectively. The density distribution of the 4-star melts are expected to merge to SAW at $\bar{r} \to 0$. For $\bar{v} < 10$, the observed exponents at short distances in the figure, $\bar{r} < 0.1$, are all less steep than that for $\bar{v} = 10$. Moreover, the distance where crossover occurs decreases as its density increases, as shown in Fig. 10(b). For instance, in the case of $\bar{\rho}_b = 10$ and $\bar{v} = 1$, the polymers hardly show any SAW. On the contrary, the intramolecular density of the star solution with $\bar{\rho}_b = 0.02$ is close to that of a dilute solution exhibiting an exponent close to SAW.

D. Structure factors of polymers in solutions and melts

The test-chain SCFT can be used to calculate the radial distribution function by holding every monomer each time and averaging by the degree of polymerization. The radial distribution for the intramolecular correlation $\omega(r)$ and the intermolecular correlation $g(r)$ of a polymer melt can be written directly as

$$\omega(r) = \frac{1}{N}\sum_{t_{\rm fix}=0}^{N} \rho^{\rm fix}(r; t_{\rm fix}) \tag{33}$$

and

$$g(r) = \frac{1}{N\rho_b}\sum_{t_{\rm fix}=0}^{N} \rho^{\rm free}(r; t_{\rm fix}). \tag{34}$$

Given a polymer melt with ρ_b and degree of polymerization N, the total structure factor is composed of both intra- and intermolecular contributions,

$$S(k) = \rho_b N\omega(k) + \rho_b^2 h(k), \tag{35}$$

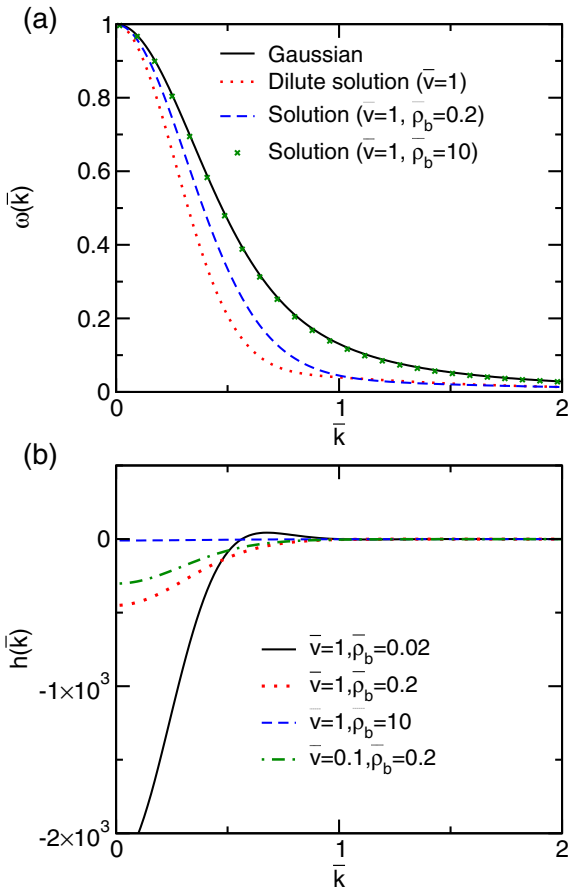

FIG. 11. Intramolecular $\omega(k)$ and intermolecular $h(k)$ structure factors of 4-star molecules ($N_{\text{star}} = 100$). The Gaussian chain is also shown in (a) for comparison.

where $\omega(k)$ is the intramolecular structure factor and $h(k)$ is the intermolecular contribution. $\omega(k)$ and $h(k)$ are three-dimensional Fourier transforms of pair correlation functions in a spherical coordinate system, $\omega(r)$ and $h(r) = g(r) - 1$. The dimensionless structure factors are written as

$$\omega(\bar{k}) = 4\pi \int_0^\infty dr \frac{\bar{r}\sin(\bar{k}\bar{r})}{\bar{k}} \omega(\bar{r}) \tag{36}$$

and

$$h(\bar{k}) = 4\pi \int_0^\infty d\bar{r} \frac{\bar{r}\sin(\bar{k}\bar{r})}{\bar{k}} (g(\bar{r}) - 1), \tag{37}$$

where $\bar{k} = kb$.

$\omega(\bar{k})$ of the 4-star molecule of the Gaussian, in a good dilute solution, in a semidilute solution with $\bar{\rho}_b = 0.2$, and in a melt with $\bar{\rho}_b = 10$, respectively, are shown in Fig. 11(a). In homogeneous melts, (e.g., $\bar{\rho}_b = 10$), $\omega(\bar{k})$ is similar to the profile of a Gaussian chain. $\omega(\bar{k})$ in a semidilute solution is intermediate between that in the dilute solution and that in the ideal chain, reflecting a partially swollen conformation. In Fig. 11(b), the intermolecular structure factors $h(\bar{k})$ in four typical 4-star solutions are shown. In the case of $\bar{\rho}_b = 10$, $h(\bar{k})$ is almost 0, indicating the absence of intermolecular correlations in high-density melts. Figure 12 shows the total static structure factors of the 4-star molecules in different

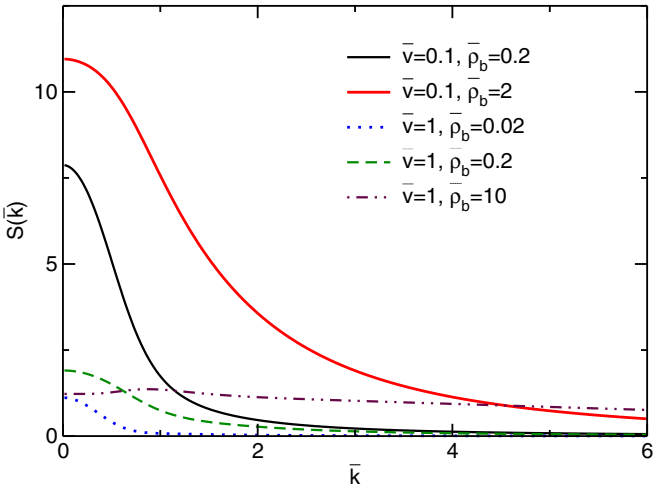

FIG. 12. Static structure factors of 4-star polymers with $N_{\text{star}} = 100$ in different solutions.

solutions. The peaks at low $\bar{k}$ in the case of $\bar{v} = 1$ and $\bar{\rho}_b = 10$ correspond to melts with a high bulk density and strong contribution of intermolecular structure factors, $\rho_b^2 h(\bar{k})$. The result shows that a peak in $S(\bar{k})$ depends only on $\bar{\rho}_b$, and not on $\bar{v}$. This theoretical prediction has not been observed in SANS experiments for homogeneous polymer melts or blends, and it remains an interesting question to explain the results of the test-chain SCFT $S(k)$ at high densities.

IV. CONCLUSION

A test-chain SCFT is presented to study polymer conformations of linear and branched polymers under various conditions. The results of linear polymers are in good agreement with classic polymer theory and simulation results [52,56]. We summarize our findings as follows.

(i) The density profile of polymers from dilute solutions to melts strongly depends on the excluded volume, $\bar{v}$. In dilute solutions, the conformation of a linear polymer is Gaussian when $\bar{v} < 0.1$. The conformation is smoothly swollen with increasing v. When $\bar{v} > 1$, the conformation can be identified as SAW. The conformations of branched polymers exhibit analogous behaviors.

(ii) The calculations successfully capture a crossover regime from SAW to Gaussian in semidilute solutions and melts at a correlation length that decreases as $\bar{v}$ increases. The Gaussian regime is vanishing as $\bar{v}$ approaches 100. Moreover, the correlation length where the crossover occurs decreases as its density increases.

(iii) Branching enhances the swelling of polymers under all conditions, especially in the regimes close to the branching point.

Finally, we emphasize that the test-chain theory is not limited to any particular cases in this work. It is rather a universal means to modeling a broad variety of polymer systems [18,57–61]. The algorithm presented here is to generalize a solution to model polymers with various architectures within the framework of one theory. This theory can be used to describe the polymer conformation and behaviors in many other complex environments with a broad range of polymer concentrations [17,60,62–65].

ACKNOWLEDGMENTS

We gratefully acknowledge Prof. Mark Foster for fruitful discussions. The research was funded by the National Science Foundation (Grant No. CBET-0731319). Numerical computations were partially supported by the Colorado School of Mines High Performance Computing Group. D.W. thanks the National "The Thousand Talents Plan" for Young Professionals for support.

[1] H. Hsieh and R. P. Quirk, *Anionic Polymerization: Principles and Practical Applications* (Marcel Dekker, New York, 1996).
[2] L. A. Archer and S. K. Varshney, Macromolecules **31**, 6348 (1998).
[3] T. D. Martter, M. D. Foster, T. Yoo, S. Xu, G. Lizzaraga, R. P. Quirk, and P. D. Butler, Macromolecules **35**, 9763 (2002).
[4] J. S. Lee, R. P. Quirk, M. D. Foster, K. M. Wollyung, and C. Wesdemiotis, Macromolecules **37**, 6385 (2004).
[5] J. S. Lee, R. P. Quirk, and M. D. Foster, Macromolecules **38**, 5381 (2005).
[6] M. G. McKee, S. Unal, G. L. Wilkes, and T. E. Long, Prog. Polym. Sci. **30**, 507 (2005).
[7] H. Gao and K. Matyjaszewski, Macromolecules **39**, 4960 (2006).
[8] Y. Chen, Z. Shen, E. Barriau, H. Kautz, and H. Frey, Biomacromolecules **7**, 919 (2006).
[9] J. Yoo, M. B. Runge, and N. B. Bowden, Polymer **52**, 2499 (2011).
[10] D. Wang, L. Pevzner, C. Li, K. Peneva, C. Y. Li, D. Y. C. Chan, K. Müllen, M. Mezger, K. Koynov, and H.-J. Butt, Phys. Rev. E **87**, 012403 (2013).
[11] S.-f. Wang, S. Yang, J. Lee, B. Akgun, D. T. Wu, and M. D. Foster, Phys. Rev. Lett. **111**, 068303 (2013).
[12] J. S. Lee, N.-H. Lee, S. Peri, M. D. Foster, C. F. Majkrzak, R. Hu, and D. T. Wu, Phys. Rev. Lett. **113**, 225702 (2014).
[13] W. Burchard, Adv. Polym. Sci. **48**, 1 (1983).
[14] A. T. Boothroyd, G. L. Squires, L. J. Fetters, A. R. Rennie, J. C. Horton, and A. M. B. G. De Vallera, Macromolecules **22**, 3130 (1989).
[15] B. Hammouda, R. M. Briber, and B. J. Bauer, Polymer **33**, 1785 (1992).
[16] B. Hammouda, Sans from homogeneous polymer mixtures: A unified overview, in *Polymer Characteristics*, Advances in Polymer Science, Vol. 106 (Springer, Berlin, Heidelberg, 1993), pp. 87–133.
[17] B. Hammouda, Polym. Rev. **50**, 14 (2010).
[18] J. S. Lee, M. D. Foster, and D. T. Wu, Macromolecules **39**, 5113 (2006).
[19] T. P. Russell, L. J. Fetters, J. C. Clark, B. J. Bauer, and C. C. Han, Macromolecules **23**, 654 (1990).
[20] C. C. Greenberg, M. D. Foster, C. M. Turner, S. Corona-Galvan, E. Cloutet, R. P. Quirk, P. D. Butler, and C. Hawker, J. Polym. Sci. Part B: Polym. Phys. **39**, 2549 (2001).
[21] B. Farnoux, F. Boue, and J. Cotton, J. Phys. (France) **39**, 77 (1978).
[22] P. G. De Gennes, *Scaling Concepts in Polymer Physics*, 1st ed. (Cornell University Press, Ithaca, NY, 1979).
[23] M. Daoud and J. Cotton, J. Phys. (France) **43**, 531 (1982).
[24] G. S. Grest, K. Kremer, and T. A. Witten, Macromolecules **20**, 1376 (1987).
[25] Y. Rouault and O. V. Borisov, Macromolecules **29**, 2605 (1996).
[26] I. Carmesin and K. Kremer, Macromolecules **21**, 2819 (1988).
[27] H. P. Deutsch and K. Binder, J. Chem. Phys. **94**, 2294 (1991).
[28] A. Yethiraj, J. Chem. Phys. **125**, 204901 (2006).
[29] A. Di Cecca and J. J. Freire, Macromolecules **35**, 2851 (2002).
[30] E. Helfand and Y. Tagami, J. Chem. Phys. **57**, 1812 (1972).
[31] E. Helfand and Y. Tagami, J. Chem. Phys. **56**, 3592 (1972).
[32] D. G. Walton and A. M. Mayes, Phys. Rev. E **54**, 2811 (1996).
[33] D. T. Wu and G. H. Fredrickson, Macromolecules **29**, 7919 (1996).
[34] D. T. Wu, G. H. Fredrickson, and J.-P. Carton, J. Chem. Phys. **104**, 6387 (1996).
[35] G. J. Fleer, M. A. C. Stuart, J. M. H. M. Scheutjens, T. Cosgrove, and B. Vincent, *Polymers at Interfaces* (Chapman and Hall, London, 1993).
[36] P. G. Ferreira and L. Leibler, J. Chem. Phys. **105**, 9362 (1996).
[37] G. Fredrickson, *The Equilibrium Theory of Inhomogeneous Polymers* (Oxford University Press, Oxford, UK, 2006).
[38] M. W. Matsen, in *Soft Matter*, edited by G. Gompper and M. Schick (Wiley-VCH Verlag, Weinheim, Germany, 2006), Vol. 1.
[39] O. V. Rud, A. A. Polotsky, T. Gillich, O. V. Borisov, F. A. M. Leermakers, M. Textor, and T. M. Birshtein, Macromolecules **46**, 4651 (2013).
[40] J. G. Curro and K. S. Schweizer, Macromolecules **20**, 1928 (1987).
[41] K. Schweizer and J. Curro, Adv. Polym. Sci. **116**, 319 (1994).
[42] C. J. Grayce, A. Yethiraj, and K. S. Schweizer, J. Chem. Phys. **100**, 6857 (1994).
[43] C. J. Grayce and K. S. Schweizer, Macromolecules **28**, 7461 (1995).
[44] D. G. Gromov and J. J. de Pablo, J. Chem. Phys. **103**, 8247 (1995).
[45] A. Yethiraj, J. Chem. Phys. **108**, 1184 (1998).
[46] R. Patil, K. S. Schweizer, and T.-M. Chang, Macromolecules **36**, 2544 (2003).
[47] J. M. H. M. Scheutjens and G. J. Fleer, J. Phys. Chem. **83**, 1619 (1979).
[48] J. Klein Wolterink, F. A. M. Leermakers, G. J. Fleer, L. K. Koopal, E. B. Zhulina, and O. V. Borisov, Macromolecules **32**, 2365 (1999).
[49] J. Klein Wolterink, J. van Male, M. A. Cohen Stuart, L. K. Koopal, E. B. Zhulina, and O. V. Borisov, Macromolecules **35**, 9176 (2002).
[50] S. F. Edwards, Proc. Phys. Soc. **88**, 265 (1966).
[51] S. F. Edwards, Proc. Phys. Soc. **85**, 613 (1965).
[52] L. R. Hutchings, R. W. Richards, S. W. Reynolds, and R. L. Thompson, Macromolecules **34**, 5571 (2001).
[53] J. des Cloizeaux, Phys. Rev. A **10**, 1665 (1974).
[54] M. Bishop, J. H. R. Clarke, A. Rey, and J. J. Freire, J. Chem. Phys. **95**, 4589 (1991).
[55] S. Caracciolo, M. S. Causo, and A. Pelissetto, J. Chem. Phys. **112**, 7693 (2000).
[56] J. C. Horton, G. L. Squires, A. T. Boothroyd, L. J. Fetters, A. R. Rennie, C. J. Glinka, and R. A. Robinson, Macromolecules **22**, 681 (1989).

[57] D. Wang, Y. Yuan, Y. Mardiyati, C. Bubeck, and K. Koynov, Macromolecules **46**, 6217 (2013).
[58] J. S. S. Wong, L. Hong, S. C. Bae, and S. Granick, Macromolecules **44**, 3073 (2011).
[59] C. Gerstl, G. J. Schneider, W. Pyckhout-Hintzen, J. Allgaier, S. Willbold, D. Hofmann, U. Disko, H. Frielinghaus, and D. Richter, Macromolecules **44**, 6077 (2011).
[60] B. McCulloch, V. Ho, M. Hoarfrost, C. Stanley, C. Do, W. T. Heller, and R. A. Segalman, Macromolecules **46**, 1899 (2013).
[61] D. Wang, R. Hu, J. N. Mabry, B. Miao, D. T. Wu, K. Koynov, and D. K. Schwartz, J. Am. Chem. Soc. **137**, 12312 (2015).
[62] T. G. Desai, P. Keblinski, S. K. Kumar, and S. Granick, J. Chem. Phys. **124**, 084904 (2006).
[63] T. G. Desai, P. Keblinski, S. K. Kumar, and S. Granick, Phys. Rev. Lett. **98**, 218301 (2007).
[64] D. Mukherji, C. M. Marques, and K. Kremer, Nat. Commun. **5**, 4882 (2014).
[65] A. Chremos, E. Glynos, and P. F. Green, J. Chem. Phys. **142**, 044901 (2015).